

UNIVERSITAT POLITECNICA DE CATALUNYA

DEPARTAMENT D'ENGINYERIA ELECTRONICA

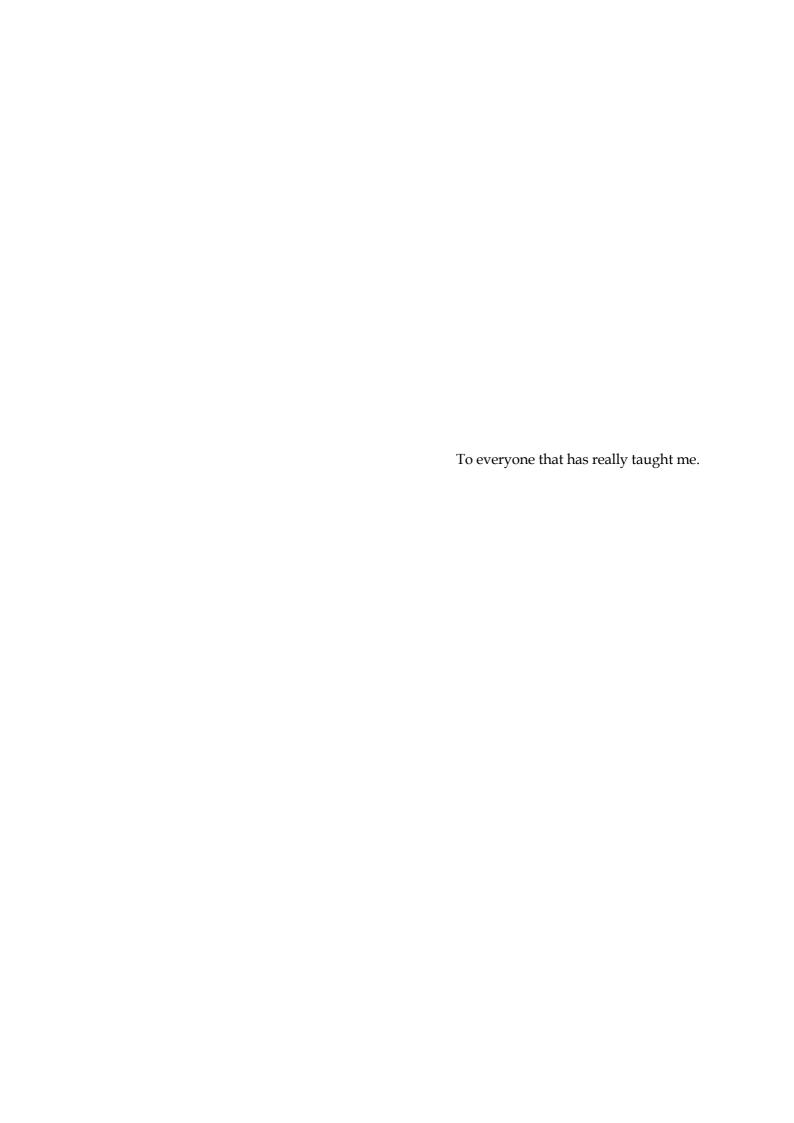
"SCENE SEGMENTATION USING NEUROMORPHIC NETWORKS"

Thesis Dissertation Submitted in Partial Fulfillment of the Requirements for the Degree of Doctor of Philosophy

Jordi Cosp Vilella

Advisor: Jordi Madrenas

July 2002



ACKNOWLEDGEMENTS

I would like to thank Dr. Jordi Madrenas, my advisor, for his continuous support and availability on the development of this thesis especially because he has never been too busy to answer my multiple questions in spite of his numerous obligations.

Many thanks to my colleagues at Electronic Engineering Department at Universitat Politècnica de Catalunya (too many to be listed here!), for sharing their opinions and knowledge on electronics and other fields. Thanks in particular to Dr. Joan Cabestany for his support and Dr. Eduard Alarcón for many useful comments on obscure aspects on electronic design.

Thanks also to Dr. DeLiang L. Wang for his helpful suggestions on many tricky features of LEGION algorithm

Last but not least, I thank my parents, Martí and Carme, and my sister Montserrat for their financial and emotional support throughout many years. Finally, I would like to thank my wife Pilar for her inconditional support during the last years and for being a constant inspiration for my life.

FUNDING

This thesis has been partially funded by CICYT projects "Arquitecturas VLSI Mixtas de Bajo Consumo para Aplicaciones Neuro-Fuzzy" (TIC96-1195), and "Sistema VLSI Analógico Bioinspirado para Segmentación de Imagen" (TIC-2001-2183) of Ministerio de Ciencia y Tecnología (Spanish Government)

This thesis has been partially funded by studentship 1997FI 00642 PG UPC of Comissionat per a Universitats i Recerca (Generalitat de Catalunya)

ABSTRACT

Advances in neurosciences have induced the development of complex models of artificial neurons closer to their biological counterparts. These models improved functionality of artificial neural networks and novel applications have appeared. Nevertheless, complexity of new neuron models makes their simulation difficult, and time and power consuming. This is not a major drawback for applications that have no restrictions on power consumption and system complexity as simulation of natural neurons or exploration of different abilities of artificial neural networks. But, there are other applications, as found in real time portable systems, that require fast and small systems and low power requirements for which simulating complex artificial neurons is not a good solution. Finding a feasible solution to this problem is the aim of this work.

This dissertation describes and analyzes a hardware model of an artificial neural network based on coupled oscillators that have been adapted to fit VLSI requirements and its applications to scene segmentation tasks. To reduce area overhead and power consumption, neurons, which are modeled as astable oscillators, are implemented on a full custom ASIC instead of being simulated on a standard hardware architecture. The implementation of a physical oscillator instead of their simulation, allows the system to perform the same tasks and reduce power consumption compared to requirements needed for a computer to simulate the network.

First, a current-mode astable oscillator is modeled as an integrator and a hysteresis comparator. Then, this scheme is used to study algebraically and numerically the synchronization of excitatory coupled oscillators with and without external inhibition and mismatch. After this, the analysis is repeated with an improved model composed of two integrators with different timescales. This allows us to simulate secondary effects as oscillator output capacitance. From these results, the behavior of one-dimensional and two-dimensional arrays of coupled oscillators is studied and then, the network is applied to synthetic image segmentation.

Based on results of the mathematical analysis, a microelectronic network is designed on a double-poly 0.8µm CMOS ASIC. This circuit is described and extensively simulated to check its functionality as a segmentation layer. Then, experimental results validate the network functionality as a segmentation network and confirm the importance of secondary effects modeled in the mathematical analysis section. Finally, this dissertation ends with an estimation of the scheme complexity, compares it to other methods, sets out concluding remarks and explores future trends on implementation of neuromorphic segmentation schemes.

Mathematical analysis and simulations demonstrate that astable oscillators can be used as basic cells of segmentation networks. They also demonstrate that delays due to cell output capacitance combined with device mismatch have to be limited below certain boundaries for the network to work properly. The physical implementation of a

neuron model based on a non-linear oscillator demonstrates that it is possible to implement an oscillatory segmentation scheme that runs much faster that its simulated counterpart on powerful computers.

Future lines of research are the deeper study of synchronization mechanisms with weaker coupling strength combined with device mismatch, the use of faster current comparators with low power consumption figures and the use of gray level input images.

TABLE OF CONTENTS

Acl	knov	vledge	ements	iii
Fur	ndin	g		iv
Ab	strac	t		v
Tak	ole o	f Cont	ents	vii
Lis	t of 1	Figures	S	x
Lis	t of T	Γables		xvii
Lis	t of 1	Publica	ations	xviii
Ι	IN	rod	UCTION	1
	I.1	Neur	omorphic Engineering	2
	I.2	The V	ision Problem	3
	I.3	Comr	mon Scene Segmentation Techniques	5
		I.3.1	Edge Detection Schemes	6
		I.3.2	Region Segmentation Schemes	8
		I.3.3	Color images	10
	I.4	Biolog	gical Principles of Oscillatory Neural Networks	10
	I.5	Oscill	latory Segmentation Schemes	12
		I.5.1	Introduction	12
		I.5.2	Malsburg's model	12
		I.5.3	LEGION	13
		I.5.4	Other Oscillatory models	15
		I.5.5	Cellular Neural Networks	16
	I.6	Neur	omorphic Vision Implementations	16
		I.6.1	Phototransduction	17
		I.6.2	Image Filtering	18
		I.6.3	Motion Computation	19
		I.6.4	Segmentation	19
		I.6.5	Neuron Oscillator Implementation	20
	I 7	Thesi	s Objectives and Outline	21

II	AST	ABLE	OSCILLATOR NETWORK	23
	II.1	Oscilla	tory Segmentation Scheme	. 25
	II.2 The Basic Ideal Oscillator		sic Ideal Oscillator	. 27
		III.2.1	Single Oscillator	27
		II.2.2	Two Coupled Oscillators	. 29
		II.2.3	Two Oscillators Plus Inhibitor	40
		II.2.4	Mismatch	41
	II.3	Output	t Delay Oscillator	43
		II.3.1	Coupled Oscillators	46
		II.3.2	Mismatch	49
		II.3.3	Inhibitor	51
	II.4	Netwo	rks of Coupled Oscillators	. 51
		II.4.1	Chains with no Inhibiton	52
		II.4.2	Chains with Inhibition	55
		II.4.3	2D-Blocks of Coupled Oscillators	. 56
	II.5	Segme	ntation	57
		II.5.2	The Role of the Inhibitor	. 59
	II.6	Discus	sion	61
III	MIC	CROEL	ECTRONIC DESIGN	63
	III.1	Micro	pelectronic Model	65
	III.2	Syste	m Architecture	66
	III.3	The C	Core	67
		III.3.1	Neural Oscillator	69
		III.3.2	2 Excitatory Synapses	76
	III.4	Globa	al Inhibitor	. 78
	III.5	Activ	ity Detectors	81
	III.6	Conti	rol Circuits	. 83
		III.6.1	Analog Biasing	84
		III.6.2	Pigital Control	84
	III.7	Imple	ementation	84
	III.8	Conc	lusions	86

IV	EXPERIMENTAL RESULTS	87
	IV.1 Free Oscillator Characteristics and Mismatch	88
	IV.2 Excitatory Synapse Characteristics	92
	IV.3 Measurement Output Interface	93
	IV.4 Segmentation	94
	IV.5 Delay Effects	95
	IV.6 Biasing	100
	IV.7 Image Noise	103
	IV.8 Segmentation Speed	106
	IV.9 Power Consumption	108
	IV.10 Performance Comparison	108
	IV.11 Concluding Remarks	111
\mathbf{V}	CONCLUDING REMARKS	113
	V.1. Remarks on Neuromorphic Implementations	114
	V.2. Contributions and Conclusions	116
	V.3. Applications	118
	V.4. Future Work	119
A	DELAY OSCILLATOR	121
BIE	BLIOGRAPHY	129

LIST OF FIGURES

II.1	Network structure. Each circle represents a cell. Only excitatory center cell connections and bottom line cell connections to inhibitor are shown for clarity.	26
II.2	Example of network oscillatory behavior. Oscillators 2 and 3 are associated with pixels that belong to the same object and oscillate in phase. Oscillator 1 is associated with a pixel that belongs to a different object; thus, it oscillates at the same frequency but with a different phase. Global inhibitor behavior is also shown at the lower time diagram. It is active when any oscillator in the network is active	26
II.3	Basic oscillator built of a hysteresis comparator and a damped integrator	28
II.4	Temporal behavior and orbit of a single ideal oscillator. Parameters are: γ =0.3, θ =1, p=0.9, q=0.1, k=3.33. Arrows indicate the evolution of state variables through time in the orbit. Note that two arrows indicate fast dynamics when x shifts from 0 to 1 and backwards	29
II.5	Temporal evolution of one oscillator coupled to another synchronous oscillator. y thresholds are shifted $S(\gamma)$ and $S(\gamma+\theta)$ during the active phase due to coupling. Notice that modifying thresholds only affects oscillators that shift to active during excitation and not afterwards	30
II.6	Temporal evolution of two oscillators A and B. Integrator voltage difference is not equal but they can be considered synchronized because both shift from active to silent state and vice versa simultaneously. Equivalent voltage thresholds are also depicted. Parameters used are γ =0.3, θ =1, S=0.2, q =0.1, p =0.9, k =3.33	32
II.7	Temporal evolution of two oscillators A and B. Integrator voltage difference is reduced after the first jump to the active state	33
II.8	Temporal evolution of two oscillators A and B. Integrator yB and yA difference shifts its sign after the first jump to the active state. This difference can be reduced (as depicted) or increased after first jump	34
II.9	Temporal evolution of two oscillators A and B. Integrator state variable difference ($\Delta y(t)$) does not change during the whole cycle.	35
II.10	Return map of two coupled ideal oscillators.	38
II.11	Temporal evolution of two oscillators A and B. $\Delta y(t)$ is not reduced after the first shift to the active state but only after the second jump to the silent state.	39
II.12	Temporal evolution of two oscillators A and B. $\Delta y(t)$ shifts it sign after the first jump to the active state and also increases difference Dy,	

	state always reduces this difference, leading to synchrony	40
II.13	Evolution of y state variables of two oscillators (osc. A thin line, osc. B thick line) with mismatch. They are synchronous at the beginning of the silent state and mismatch is responsible of difference y variables at the end of the same state.	42
II.14	Hysteresis oscillator with output delay modeled as two integrators with different time constants.	43
II.15	Evolution through time of x and y of a single oscillator. y-threshold values are Γ =0.3 and Γ + Θ =0.62 are also depicted with dashed lines. Note that y range is not limited to thresholds (dashed lines) in this figure neither in Figure II.16 due to output delays	45
II.16	Orbit of a single oscillator. y-threshold values (Γ =0.3 and Γ + Θ =0.62) and reference value (R=0.3) are also depicted with dashed lines	45
II.17	z' and w' vs. x plot when w <z< td=""><td>45</td></z<>	45
II.18	z' and w' vs. x plot when w>z	45
II.19	Orbit of the delay oscillator (thin line) and its simplification for analysis purposes (thick line). Thresholds have changed to Γ -D and Γ + Θ (γ)+D.	46
II.20	Simulated return map of two coupled delay oscillators (thick line) and two coupled ideal oscillators (thin line). Synchronization occurs below an initial y-difference of 0.18 approximately for both of them.	48
II.21	Variation of differences of y ($\Delta y=yA-yB$) for two coupled oscillators as a function of period mismatch ($\Delta T/T$). Oscillators have been considered synchronous at the beginning and mismatch is the only responsible of producing this difference at the steady state	50
II.22	Lag between rising edges of two coupled oscillators in function of mismatch of periods. As in Figure II.21, oscillators start synchronous and mismatch is the only responsible for the lag. As the active pulse width is 0.7s, both pulses are simultaneously active at least the 50% of this period for a 28% period mismatch	51
II.23	Temporal behavior of a 16-oscillator one-dimensional network. Thin lines mark periods when any oscillator is active. All oscillators are equal but start with different initial conditions. Note that perfect synchrony is easily achieved after few cycles	53
II.24	Temporal behavior of the same network with different initial conditions that prevent the network from synchronizing	53
II.25	Temporal behavior of a chain of oscillators with 5% mismatch in the period.	54

11.26	Temporal behavior of a chain of oscillators with 10% mismatch in the period	54
II.27	Temporal behavior of a chain of oscillators with a slow hysteresis comparator (ϵ =0.66)	54
II.28	Temporal behavior of a chain of oscillators with a low exciting parameter (s=0.25)	54
II.29	Combined effect of mismatch and different initial conditions. Parameters are the same as in Figure II.24 and Figure II.25 but the combined effect leads to synchrony.	55
II.30	Temporal evolution of a chain of oscillators with 10% mismatch and an inhibitor with strength i=0.1	56
II.31	Temporal evolution of oscillators of a 4x4 network. s=0.25, i=0.1, 10%mismatch	57
II.32	Temporal evolution of the 4x4 network. The original image to be segmented is shown at the left.	58
II.33	Network state at different instants. Vertical bars show the output level (from 0 to 1) of each oscillator.	58
II.34	Temporal evolution of the 4x4 network. The original image to be segmented is shown at the left.	59
II.35	Network state at different time instants. Vertical bars show the output level (from 0 to 1) of each oscillator	59
II.36	Temporal evolution of the 4x4 network of Figure II.34 with high mismatch (25%) and stronger excitatory coupling (s=1.5). Note that frequency of oscillators mapped to the background (object 3) is higher than other oscillators. This leads to the fact that object 2 and background oscillators are active simultaneously and cannot be distinguished at time t=70.	61
III.1	Oscillator modeled as dependent current sources.	65
III.2	System architecture. The 16x16 oscillator core is surrounded by the global inhibitor, digital control, analog biasing, direct outputs of some oscillators and boundary circuits to cancel boundary synapses	67
III.3	Diagram of four core elements. Each cell has 1 oscillator, 4 synapse circuits and two XNOR gates that are shared between adjacent cells. Memory elements and their connections to digital gates are not shown for clarity.	68
III.4	Digital architecture of the network. Only four cells of the bottom-right corner are presented. Note inverters in the right boundary that force a 0 output of the XNOR gates and the direct connections to ground on the bottom boundary to switch off synapses.	69

III.5	Basic oscillator schematics.	70
III.6	Temporal evolution of Vout and Vint voltages of the basic oscillator	72
III.7	Oscillator orbit and static voltage thresholds: V(Ipos) as M1 and V(Ipos+Iwid) as (M2)	72
III.8	Oscillator orbit when Iwid is increased (Iwid=2.5µA)	73
III.9	Oscillator frequency and duty cycle as a function of Iwid	73
III.10	Oscillator orbit when Ipos is increased (Ipos=1µA)	74
III.11	Oscillator frequency and duty cycle as a function of Ipos	74
III.12	Oscillator orbit when Ichr decreases (Ichr=333nA)	75
III.13	Oscillator frequency and duty cycle as a function of Ichr	75
III.14	Oscillator orbit when Ides increases (Ides=333nA)	76
III.15	Oscillator frequency and duty cycle as a function of Ichr	76
III.16	Excitatory synapse schematic	77
III.17	XNOR gate	77
III.18	Excitatory synapse current activity (thick lines) for different biasing values when a neighbor cell output voltage (thin line) switches to active. Note that excitatory synapse becomes active during the switching time of the output voltage; thus, the former delay can be modeled as a slight modification of the reference voltage.	78
III.19	Global inhibitor cell	79
III.20	Discharging time delay of Vact node (thin lines) for different pull-up Ia current biasing (from 1mA to 100mA) and an oscillator like input (thick line)	81
III.21	Activity detection circuit for 1 column. The block depicted on the right is cloned in each cell.	82
III.22	Activity detector response (thin line) to selection pulse (thick line) with different pull-up biasing currents (from 10mA to 100mA)	83
III.23	Microphotograph of the complete circuit. We indicate different components of the design.	85
III.24	Microphotograph of a single cell with its different parts. Biasing connections can be easily distinguished on each side of the photograph and the integrator capacitor on the upper left corner	85
IV.1	Period of each oscillator of the network under two different biasing conditions (top and bottom). Differences between oscillators (x-axis) are larger than differences between different experiments with the same oscillators (height of each vertical line)	88

IV.2	Ratio between standard deviation and mean value of period of 256 non-connected oscillators as a function of different biasing values
IV.3	Oscillator frequency as a function of Ipos current biasing. Experimental results: solid line. Simulated results: dashed line
IV.4	Oscillator frequency as a function of Iwid current biasing. Experimental results: solid line. Simulated results: dashed line
IV.5	Oscillator frequency as a function of Ides current biasing. Experimental results: solid line. Simulated results: dashed line
IV.6	Oscillator frequency as a function of Ichr current biasing. Experimental results: solid line. Simulated results: dashed line
IV.7	Mean delay between cells of a chain of coupled oscillators as a function of excitatory current
IV.8	Input image mapped to oscillators (top) and network state at 4 different timesteps (bottom). Black pixels represent active oscillators and white pixels silent oscillators
IV.9	Activity of oscillators of the first row of the image. Pixels number 0, 1 and 5 to 14 are mapped to background. Pixels 2 to 4 are mapped to the cross and pixel 15 to the arrow.
IV.10	Background oscillator activity (channel 1, top) and activity detector response (channel 2, bottom) as seen in an oscilloscope. Note that four activity detector cycles occur at each basic oscillator cycle
IV.11	Delay of indirectly connected oscillators. Oscillator #1 and #2 are directly connected and their delay is τ , while delay between oscillators #1 and #5, which are not directly connected, is τ' that is bigger than τ . The activity detector waveform is also shown at the top96
IV.12	Input spiral (top) and network state at different timesteps (mid and lower rows). Black pixels represent active oscillators; white pixels and gray pixels, silent oscillators. Gray is used for clarity to indicate the object to which belong active pixels. Since only some timesteps are shown, some pixels do not appear as active in any plot although the network properly segments the image
IV.13	Oscillator (channel 1, top) and activity detector (channel 2, bottom) when input image is spiral in top of Figure IV.12
IV.14	Input image (top) and network state at different timesteps (lower rows). Black pixels represent active oscillators; white pixels and gray pixels, silent oscillators. Gray is used for clarity to indicate the object to which active pixels belong.
IV.15	Activity of the 9th oscillator row (015) plus global inhibitor (16) for image in Figure IV.14
IV.16	Input image

IV.17	Activity of the middle row when Ides is 45nA	101
IV.18	Activity of the middle row for a greater Ides (75nA)	101
IV.19	Activity of the middle row for Ides=250nA	102
IV.20	Activity of the middle row when Ides is very small (15nA). To check frequency, observe at the lower left corner inhibitor activity of the previous period.	102
IV.21	Activity of the middle row for low inhibition biasing (Iinh=20nA)	102
IV.22	Activity of the middle row for high inhibition biasing (Iinh=820nA)	102
IV.23	Activity of the middle row for low excitatory currents (Iexc=500nA)	103
IV.24	Activity of the middle row for high excitatory currents (Iexc=3.5µA)	103
IV.25	Activity of the network for very small position biasing (Ipos=1nA)	103
IV.26	Activity of the network for high position biasing (Ipos=2500nA)	103
IV.27	Input noisy image (top) and active oscillators (bottom) during four different temporal slots in each period	104
IV.28	Activity of row number 5 for input image of Figure IV.27 and Ipos=50nA	105
IV.29	Activity of row number 5 for input image of Figure IV.27 and Ipos=150nA	105
IV.30	Noisy input image (top) and network state during four different temporal slots during one oscillator period	105
IV.31	Background oscillator activity (top) and inhibitor activity (bottom) for input image in Figure IV.30. The length of each inhibitor pulse displays complexity of each object. The shortest belongs to letter 'C' and the widest to the background.	106
IV.32	Synchronization of two coupled oscillators. Excitatory coupling (Iexc=500nA) is established at triggering signal (indicated by letter T in the image) and synchrony is rapidly achieved after one cycle	107
IV.33	Synchronization of two coupled oscillators. Mismatch forces slow synchronization. Excitatory coupling is weak (Iexc=50nA) and established at triggering signal indicated by T. Two oscilloscope images with different delay are shown to appreciate the whole synchronization process.	
IV.34	Synchronization of a line of oscillators. Before triggering, indicated by a t and a vertical dotted line after the first period, there are two uncoupled lines of eight oscillators. After triggering, a 500nA excitatory current couples both lines and synchrony is achieved after two cycles	108

A.1	Temporal evolution of the	ne delay oscillator	during one cycle with i	ts
	different six zones			121

LIST OF TABLES

III.1	Bias parameters used in this section.	71
IV.1	Mean standard deviation of periods for different oscillators and different experiments.	89
IV.2	Biasing conditions in Figure IV.2	90
IV.3	Biasing currents and voltages for Figure IV.8, Figure IV.9 and Figure IV.10.	94
IV.4	Bias currents and voltages for image in Figure IV.14	98
IV.5	Biasing currents and corresponding power consumption and operating frequency for 3.3V power supply	108
IV.6	Execution time of various oscillatory segmentation network implementations	109

LIST OF PUBLICATIONS

- J.Cosp, J.Madrenas. Scene Segmentation Using Neuromorphic Networks. IEEE Transactions on Neural Networks. *Submitted*
- J.Cosp, J.Madrenas. A Microelectronic Implementation of a Bioinspired Analog Matrix for Object Segmetation of aVisual Scene. 9th European Symposium on Artificial Neural Networks (ESANN'2001), pp. 69-74, 2001
- J.Cosp, J.Madrenas. A Neural Network for Scene Segmentation Based on Compact Astable Oscillators. 9th Int. Conf. on Artificial Neural Networks (ICANN99), pp.690-695, 1999
- J.Cosp, J.Madrenas. A Compact Astable Oscillator Network for Scene Segmentation. XIV Design of Circuits and Integrated Systems Conference. (DCIS'99), pp.163-167, 1999
- J.Cosp, J.Madrenas, J.Cabestany. A VLSI Implementation of a Neuromorphic Network for Scene Segmentation. 7th Int. Conf. on Microelectronics for Neural, Fuzzy and Bio-Inspired Systems (MicroNeuro'99). pp.403-408, 1999
- J.Cosp, J.Madrenas, J.M.Moreno, J.Cabestany. Analog VLSI Implementation of a Relaxation Oscillator for Neuromorphic Networks. *in Neuromorphic Systems: Engineering Silicon from Neurobiology, pp.*197-208, 1998